Pressure-dependent structural and electronic properties of quasi-one-dimensional $(TMTTF)_2PF_6$

E Rose[1], C Loose[2], J Kortus[2], A Pashkin[3,4], C A Kuntscher[3], S G Ebbinghaus[5], M Hanfland[6], F Lissner[7], Th Schleid[7] and M Dressel[1]

[1] 1. Physikalisches Institut, Universität Stuttgart, Pfaffenwaldring 57, 70550 Stuttgart, Germany
[2] Institut für Theoretische Physik, TU Bergakademie Freiberg, Leipziger Straße 23, 09599 Freiberg, Germany
[3] Experimentalphysik II, Universität Augsburg, Universitätsstraße 1, 86159 Augsburg, Germany
[4] Institut für Physik, Universität Konstanz, Universitätsstraße 10, 78464 Konstanz, Germany
[5] Martin-Luther-Universität Halle-Wittenberg, Institut für Chemie, Kurt-Mothes-Straße 2, 06120 Halle, Germany
[6] European Synchrotron Radiation Facility, BP 220, 38043 Grenoble, France
[7] Institut für Anorganische Chemie, Universität Stuttgart, Pfaffenwaldring 55, 70550 Stuttgart, Germany

E-mail: dressel@pi1.physik.uni-stuttgart.de

Abstract

We have performed detailed x-ray investigations of the quasi-one-dimensional organic conductor $(TMTTF)_2PF_6$ at room temperature and hydrostatic pressures up to 27 kbar. Based on the pressure-dependent crystal structure, the electronic band structure was calculated by density functional theory (DFT). Our systematic study provides important information on the coupling among the organic molecules but also to the anions. We discuss the consequences for the electronic properties and compare them with optical investigations under pressure. The increasing plasma frequency observed perpendicular to the stacks corresponds to a widening of the bands for the *b*-direction. Around 20 kbar a dimensional crossover occurs from a one-dimensional Mott insulator to a two-dimensional metal.

1. Introduction

In the last couple of years, the Fabre salts $(TMTTF)_2X$ and Bechgaard salts $(TMTSF)_2X$ have been established as model systems to investigate physics in reduced dimensions since they provide the unique possibility of exploring the physical properties as a function of dimensionality by tuning via chemical or physical pressure. These quasi-one-dimensional organic compounds are charge-transfer salts consisting of stacks of the planar organic molecules TMTTF (which stands for tetramethyltetrathiafulvalene) or TMTSF (tetramethyltetraselenafulvalene) along the *a*-axis that are separated in the *c*-direction by monovalent anions, such as centrosymmetric AsF_6^-, PF_6^-, SbF_6^-, Br^-, or tetrahedral ReO_4^-, ClO_4^-. In the *b*-direction the distances of the stacks are comparable to the van der Waals radii [1–3]. According to stoichiometry, $(TMTTF)_2X$ and $(TMTSF)_2X$ salts should form metallic compounds with a three-quarter-filled conduction band but due their strong anisotropy and electronic interaction the systems become insulating upon cooling. What was considered disappointing at the beginning in fact contains most exciting physics: the families of Fabre and Bechgaard salts have been at the focus of enormous scientific effort during the last three decades because small variations of the molecules or moderate pressure tune the systems through several interesting ground states (cf figure 1), such as antiferromagnetic insulator, spin-Peierls state, spin-density-wave state and superconductor; furthermore one observes a crossover from a Luttinger liquid toward a Fermi-liquid metal, charge-ordered insulator and electronic ferroelectrics [4–7].

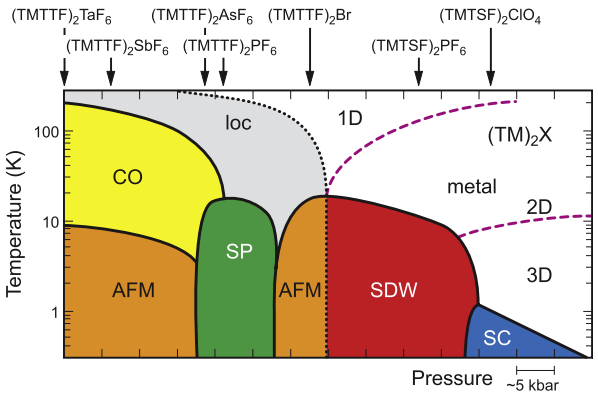

Figure 1. The phase diagram of the quasi-one-dimensional TMTTF and TMTSF salts, first suggested by Jérome and co-workers [8] and further supplemented by many groups over the years [6]. The ambient-pressure positions in the phase diagram are indicated for the different compounds with centrosymmetric anions. Going from the left to the right, the materials get less one-dimensional due to increasing interaction in the second and third directions. At low temperatures various broken symmetry ground states develop. Here loc stands for charge localization, CO for charge ordering, SP for spin-Peierls, AFM for antiferromagnet, SDW for spin-density wave, and SC for superconductor. While some of the boundaries are clear phase transitions, the ones indicated by dashed lines are better characterized as crossovers. The position in the phase diagram can be tuned by external or chemical pressure. Reproduced with permission from [36]. Copyright 2003 American Physical Society.

Here we focus on the Fabre salts that serve as prime examples of one-dimensional Mott insulators and antiferromagnetic Heisenberg chains; charge order due to electronic correlations provides the basis for a ferroelectric state. It is well known that chemical as well as physical pressure strongly influences the electronic properties, best presented in the unified phase diagram (figure 1) that relates various states to a change of dimensionality [2, 3, 5]. The paramount question is the interplay of structural and electronic properties, as can be exemplified by the shift of the charge-order transition temperature T_{CO} as pressure is applied, the transition from a charge-localized insulator to a one- or higher-dimensional metal, but also the alternation between antiferromagnetic, spin-Peierls and spin-density wave.

Over the years the crystal structures of all of these compounds have been investigated at ambient conditions [9–17]; however, only a few studies have been performed under pressure [18–24] yielding the atomic coordinates. In particular, the dimensional crossover from one-dimensional toward a more two-dimensional system has never been studied systematically with respect to changes in the crystal structure. Here we present detailed x-ray crystal data of $(TMTTF)_2PF_6$ and analysis of the data with respect to changes of the interchain coupling, dimerization and the resulting changes of the electronic band structure.

2. Experimental and numerical details

The electrochemical growth of TMTTF single crystals is described in detail in [25]. All Fabre and Bechgaard salts crystallize in the same stoichiometry and are isostructural. The planar TMTTF-molecules stack in a slight zig-zag configuration along the *a*-axis which constitutes the highest conducting direction. With some minor interaction between the stacks, they form layers in the *ab* plane, which alternate with the anions X along the *c*-axis. According to the triclinic symmetry $P\bar{1}$ (C_i), b' denotes the projection of the *b*-axis perpendicular to *a*, and c^* is normal to the *ab* plane. Recently it was pointed out that the contacts between the anions and the organic molecules via the methyl groups and the sulfur atoms are important and should not be neglected when considering the charge-order transition [4, 25]. Furthermore, the molecular stacks are not homogeneous: the TMTTF molecules form dimers with important consequences on the electronic properties of these salts [4]. The 3/4-filled conduction band (1/4-filled hole band) is split and becomes effectively half-filled; dimerization also favors the phenomenon of charge localization.

Structural investigations under ambient conditions were performed at Universität Stuttgart using a Kappa CCD Bruker AXS diffractometer, whereas the pressure-dependent x-ray diffraction experiments were carried out at beamline ID09A of the European Synchrotron Radiation Facility in Grenoble. The wavelength used for the latter experiments was 0.413 Å and the diffraction angle θ was about 25°. X-ray diffraction patterns were collected on an imaging plate MAR345 detector by rotating the crystal from −30° to +30° with 2° steps and were analyzed using the XDS package [26]. The refinement of the atomic positions was performed by the SHELX software within typical *R*-values of 0.07–0.08. The pressure in the diamond anvil cell was obtained by gaseous helium as pressure transmitting medium and determined *in situ* by the ruby luminescence method [27]. To consider the effects of the diamond window, reference measurements with the empty pressure cell were performed. All presented data were taken at room temperature.

Going to very high pressure up to 100 kbar structural phase transitions from triclinic to nearly orthorhombic phase are observed at 55 and 85 kbar in $(TMTSF)_2PF_6$ and $(TMTTF)_2PF_6$, respectively [24]. In order to avoid this complication, here we restrict ourselves to pressure values below 30 kbar.

The band structure calculations were performed using density functional theory (DFT) as implemented in PWscf-code [28]. For the exchange–correlation functional a generalized gradient approximation due to Perdew *et al* [29] together with a set of ultrasoft pseudopotentials was used. The plane wave basis set was determined by the kinetic energy cut-off at 408 eV. For the calculations, the experimentally obtained unit cell parameters for the different pressures were used; the atomic positions, however, were relaxed in each case using the Broyden–Fletcher–Goldfarb–Shanno (BFGS) minimization [30–33]. The BFGS method is a quasi-Newton algorithm based on the trust radius procedure and varies the position of the atoms under the constraint that the symmetry of the system is conserved.

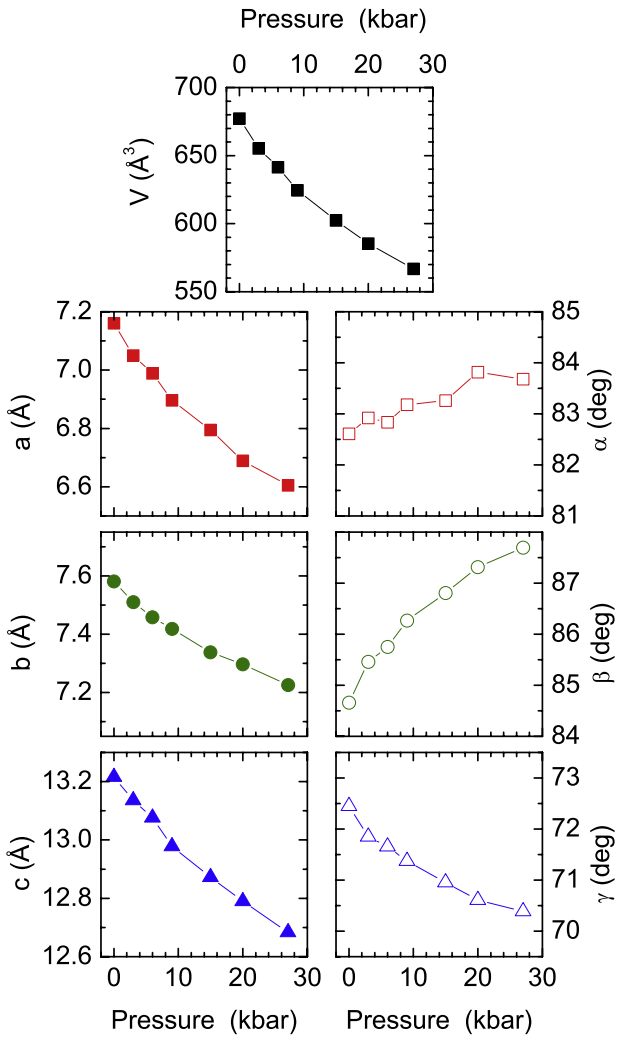

Figure 2. Change of the unit cell parameters of $(TMTTF)_2PF_6$ with increasing hydrostatic pressure measured at room temperature. V denotes the unit cell volume, a, b and c are the lattice parameters, α, β and γ are the corresponding angles of the triclinic structure. The values are listed in table 1.

3. Structural changes

Applying hydrostatic pressure entails an enormous shrinking of the unit cell volume V as demonstrated in figure 2. Whereas the unit cell volume V is 677.18 Å^3 at ambient pressure, it decreases by about 16.3% to 566.74 Å^3 at $P = 27$ kbar. This is an average reduction of the unit cell volume by about 4 Å^3 kbar^{-1} pressure, far more than for conventional metals. The main contribution to this reduction of V comes from the shortening of the a-axis by 7.1%. The decreases observed for the b- and c-axes (4.7% and 4.0%, respectively) are comparable and a bit more than half of that of the a-axis. Details are listed in table 1. In contrast, the crystal angles develop very differently under pressure. While the angle α does not change significantly (approximately 1.3%), β increases by about 3.6% and γ reduces to a smaller value with a change of 2.8%. This decrease in γ eventually triggers the high-pressure transition discovered in [24].

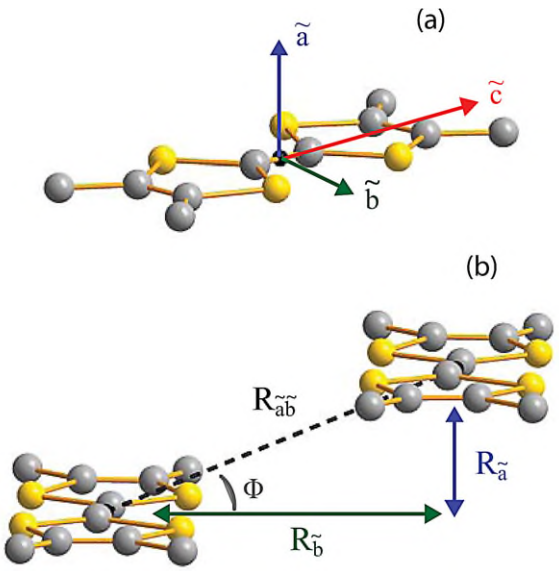

Figure 3. (a) Definition of the coordinate system $(\tilde{a}, \tilde{b}, \tilde{c})$ located in the center of gravity defined by the four sulfur atoms of the TMTTF-molecule. (b) Description of the direct distance R and its projection $R_{\tilde{a}\tilde{b}}$ onto the ab plane, the shifts $R_{\tilde{a}}$ and $R_{\tilde{b}}$ along the $\tilde{a}$-direction and along the small molecular axis $\tilde{b}$, respectively, and the angle Φ between $R_{\tilde{a}\tilde{b}}$ and $R_{\tilde{b}}$.

Table 1. Room temperature unit cell parameters of $(TMTTF)_2PF_6$ measured at different values of the hydrostatic pressure P.

P (kbar)	a (Å)	b (Å)	c (Å)	V(Å^3)
0	7.161	7.581	13.216	677.18
3	7.050	7.510	13.136	655.23
6	6.989	7.458	13.076	641.45
9	6.896	7.418	12.978	624.39
15	6.795	7.338	12.872	602.38
20	6.689	7.297	12.790	585.39
27	6.605	7.226	12.683	566.74
P (kbar)	α (deg)	β (deg)	γ(deg)	
0	82.609	84.661	72.449	
3	82.919	85.459	71.849	
6	82.837	85.752	71.656	
9	83.179	86.269	71.372	
15	83.258	86.807	70.952	
20	83.814	87.316	70.608	
27	83.678	87.695	70.388	

The change of the unit cell parameters reflects the influence of hydrostatic pressure only in a very general way and cannot account for more subtle modifications in the orbitals and orientation. It is very helpful to consider the exact relations and distances of the TMTTF-molecules with respect to each other and their changes under pressure. For this analysis the above coordinate system of the crystal axes turns out to not be appropriate, and hence we define a Cartesian coordinate system linked to the TMTTF-molecules themselves. The origin is positioned in the center of the TMTTF-molecule, defined as the center of gravity of the four sulfur atoms, as shown in figure 3. The $\tilde{a}$-axis is normal to the molecular plane and deviates a few degrees from the

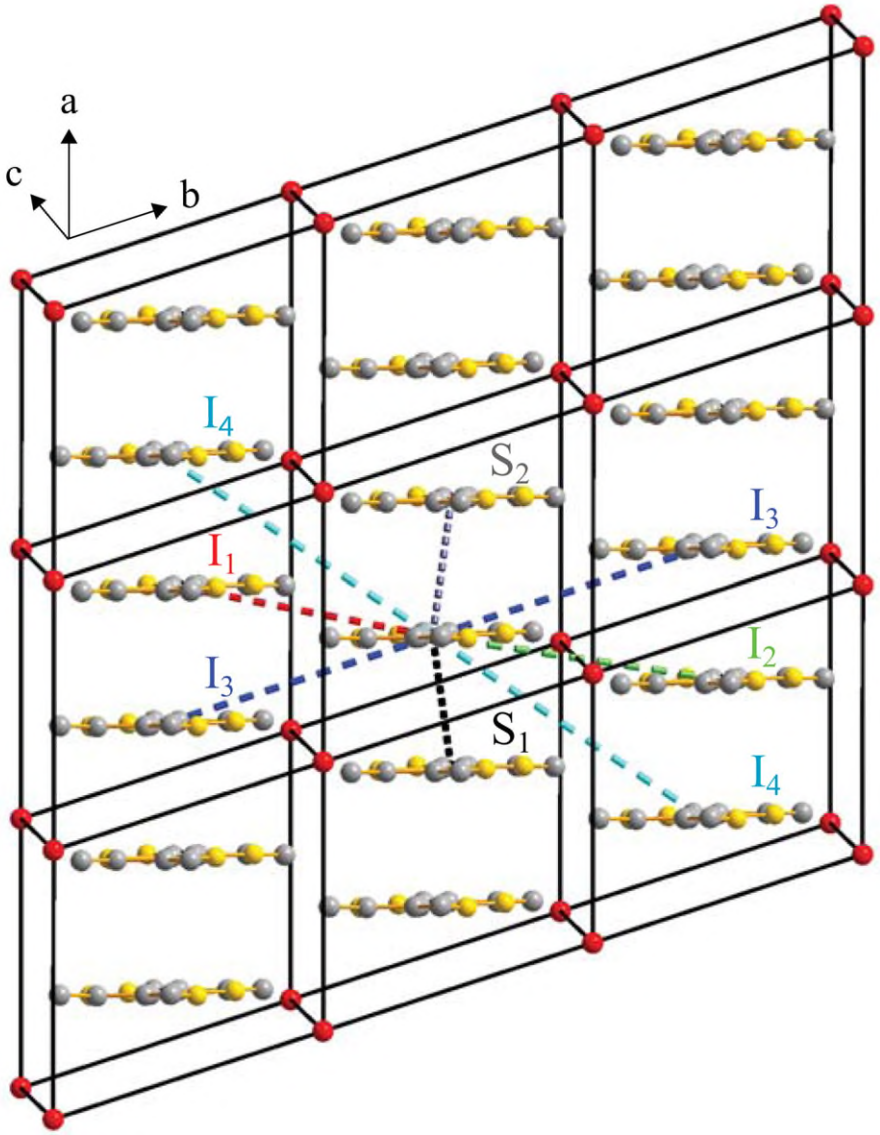

Figure 4. View of the *ab* plane of $(TMTTF)_2PF_6$ with the relevant contacts to the neighboring TMTTF-molecules along the stacks (S_1 and S_2) and to the neighboring stacks in the *b*-direction (I_1, I_2, I_3 and I_4). The positions of the anions are indicated by the red spheres.

stacking direction, while the $\tilde{c}$-axis points along the longest molecule extension. The direction $\tilde{b}$ is in line with the small molecular axis. In the following all distances between TMTTF-molecules are specified as the separations of the centers of the molecules with respect to each other, if not stated otherwise.

With respect to this new coordinate system, the direct distance R between the centers of gravity of the different neighboring TMTTF-molecules can be specified. Upon applying pressure the unit cell shrinks and all distances within the stacks and toward all neighboring stacks in the b and c-directions decrease (figure 5). However, the exact positions of the TMTTF-molecules with respect to each other are also relevant, e.g. their shifts along the small or long molecular axes ($\tilde{b}$- or $\tilde{c}$-directions) and their distances along the stacking direction ($\tilde{a}$-direction). We introduce $R_{\tilde{a}}$, $R_{\tilde{b}}$ and $R_{\tilde{c}}$ as the respective projections onto the $\tilde{a}$, $\tilde{b}$ and $\tilde{c}$-axes. All of these parameters influence the physical properties, e.g. the transfer integrals and consequently the band structure. They are described in the following subsections separately, depending on their relative positions.

3.1. Changes within the stacks (a-direction)

Along the stacking direction, the $(TMTTF)_2X$ salts are dimerized, i.e. the distances S_1 and S_2 (figures 5(a) and 6(a)) are slightly different; the dimerization changes with pressure. Two main contributions to this pressure-dependent structural dimerization are relevant. Firstly, the difference in $R_{\tilde{a}}$ between the TMTTF-molecules with respect to the $\tilde{a}$-axis as displayed in figure 7(a); this describes the alternation of spacing along the stacking direction. In addition the molecules are shifted with respect to each other, described by a variation along the $\tilde{c}$-direction, shown in figure 7(b). For all investigated pressures, no relevant modification is observed for the $\tilde{b}$-direction, as indicated in the inset of figure 7.

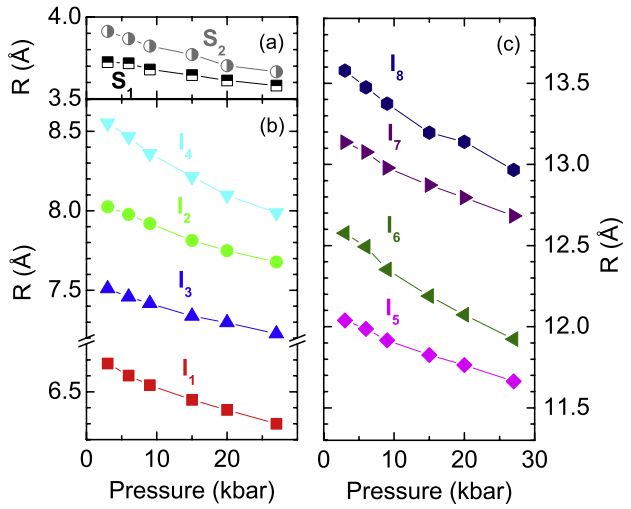

Figure 5. Direct distance R between different TMTTF-molecules, (a) for the stacking direction, (b) for coupling to neighboring stacks along the b-direction and (c) along the c-direction. The different curves are labeled according to figures 4 and 9.

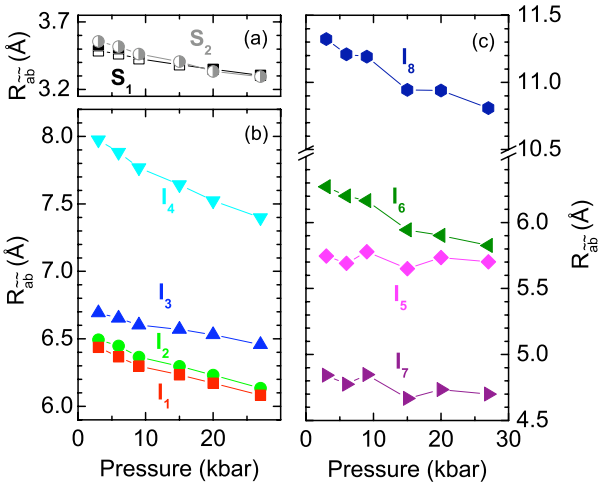

Figure 6. Projection of the distance R onto the $\tilde{a}\tilde{b}$ plane, called $R_{\tilde{a}\tilde{b}}$, between different TMTTF-molecules, (a) for the stacking direction, (b) for coupling to neighboring stacks along the b-direction and (c) along the c-direction. The definitions of the different contacts in the $(TMTTF)_2PF_6$ lattice are given in figures 4 and 9.

While $R_{\tilde{a}}$ decreases for both adjacent molecules related by S_1 and S_2, the distance $R_{\tilde{c}}$ shows the reverse tendency, as displayed in figure 7(b). If we consider the relative dimerization ΔR_i defined as

$$\Delta R_i = 2\frac{R_i(S_2) - R_i(S_1)}{R_i(S_2) + R_i(S_1)}, \qquad (1)$$

we still find a reduction of the dimerization with pressure. The relative structural dimerization $\Delta R_{\tilde{a}}$ is about ten times smaller than $\Delta R_{\tilde{c}}$, as shown in figures 7(c) and (d), respectively. At about 20 kbar the contribution $\Delta R_{\tilde{a}}$ disappears, and the spacing along the stack becomes equal.

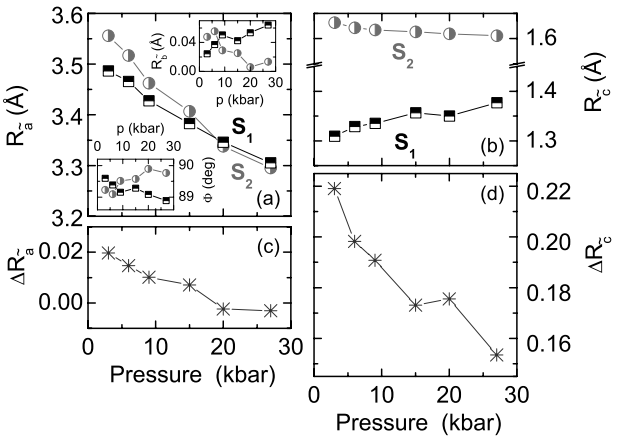

Figure 7. Parameters for the distances of neighboring TMTTF-molecules along the a-axis of $(TMTTF)_2PF_6$. (a) Under pressure the distance $R_{\tilde{a}}$ decreases for the two neighbors differently, resulting in a vanishing relative dimerization $\Delta R_{\tilde{a}}$ (panel (c)). The shifts along the $\tilde{b}$-direction and the related angle Φ are negligibly small for all pressure values, as shown in the two insets. (b) Along the molecular axis $\tilde{c}$ the relative position $R_{\tilde{c}}$ shifts in the opposite direction; (d) the resulting relative dimerization $\Delta R_{\tilde{c}}$ decreases.

3.2. Changes toward neighboring stacks in the b-direction

The distance between two TMTTF-molecules in adjacent stacks is much larger than within the stack itself. The direct distance R is in the range of 6–8 Å if one takes into account the four nearest neighbors in the b-direction. Under pressure R decreases for all four neighbors as plotted in figure 5(b). From figure 6 we see that the projection onto the $\tilde{a}\tilde{b}$ plane $R_{\tilde{a}\tilde{b}}$ exhibits a qualitatively similar dependence.

The behavior is less uniform if we analyze the changes with respect to the distances along the molecular $\tilde{b}$ and $\tilde{c}$-axis and perpendicular to them; figure 8 demonstrates this rather complex behavior. While for three neighboring molecules the distances in the stacking direction are reduced ($R_{\tilde{a}}(I_1)$, $R_{\tilde{a}}(I_2)$ and $R_{\tilde{a}}(I_4)$), the contact decreases with pressure when looking toward I_3 (figure 8(a)). This neighbor moves further away as hydrostatic pressure is applied. Accordingly the angle Φ increases with pressure as plotted in figure 8(d). When the distance along the small molecular axis $\tilde{b}$ is considered, the changes with increasing pressure are rather similar for all four neighbors (figure 8(c)). The stacks in the $\tilde{b}$-direction move closer together by about 0.35 Å when the pressure is raised to 27 kbar; this corresponds to a change of about 6%. It is interesting to consider the absolute values for the shifts $R_{\tilde{c}}$ in this regard. While the molecules connected by I_1 (closest neighbor) are shifted only by about 1.7 Å with respect to each other, a huge displacement of about 4.6 Å occurs for the second closest contact I_2. The changes of $R_{\tilde{c}}(I_3)$ and $R_{\tilde{c}}(I_4)$ are about 3.0–3.4 Å.

In addition to the reduction observed for the absolute values of the molecular distances in neighboring stacks toward the b-direction, it is important to consider the shifts of the related stacks with respect to each other. As the pressure increases, those two TMTTF-molecules that are located in neighboring unit cells but not connected by

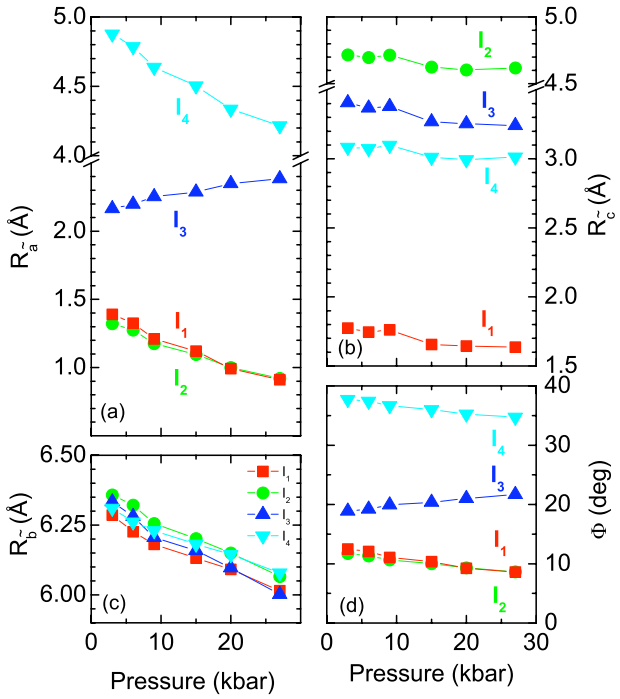

Figure 8. Distances to the four closest neighboring molecules in the b-direction labeled by I_1 through I_4 according to figure 4. (a) Distances along the stacking direction $\tilde{a}$ and (b) shift along the molecular axis $\tilde{c}$. (c) The changes with respect to the $\tilde{b}$-axis are uniform. Note, the vertical axis is scaled by a factor of 2 with respect to the upper panels. (d) Pressure-dependent changes of the angle Φ that is related to the ratio of $R_{\tilde{a}}$ and $R_{\tilde{b}}$.

translational symmetry get closer. This leads to a more parallel configuration along the b-direction and an increase in dimensionality. In [24] we have seen that for even higher pressure the structure locks into a quasi-orthorhombic configuration dominated by sheets of TMTTF-molecules.

3.3. Changes toward neighboring stacks in the c-direction

As seen from figure 5, even for neighboring stacks the absolute distance R is huge in the c-direction; the projection $R_{\tilde{a}\tilde{b}}$ onto the $\tilde{a}\tilde{b}$ plane, however, is in the same range as the one in the b-direction (figure 6). The large shift of $R_{\tilde{c}}$ along the molecular axis (figure 10) results in a very weak and almost negligible interaction between the stacks in the c-direction. For the molecules linked by I_5 to I_7 the values of $R_{\tilde{c}}$ are larger than the average extension of the molecule, which is about 8.7 Å and 3.0 Å for the large and small molecular axes, respectively. The only exception here is the connection I_8, since the related molecule belongs to the unit cell shifted by $\vec{c}$–$\vec{b}$ with respect to the reference molecule. For this molecule a relevant interaction might exist, directly or via the closest anion. Over the entire investigated pressure range the direct distance between the phosphorous and sulfur atoms P and S shrinks by about 0.7 Å, leading to closer contacts also between the two TMTTF.

Let us consider the relative positions of molecules in neighboring stacks related to each other by the lattice vector

Table 2. Band structure parameters of $(TMTTF)_2PF_6$ at different pressures. $W_X^u = \Delta E_{\Gamma\to X}^{upper}$ and $W_X^l = \Delta E_{\Gamma\to X}^{lower}$ are the bandwidths of the upper and lower bands in the stacking direction; W_X is the overall bandwidth and Δ_X denotes the gap at the X-point in the Brillouin zone. The units of the energies are in electronvolts, the calculated error is about ± 0.005 eV.

P (kbar)	E_F	W_X^u	W_X^l	W_X	Δ_X
3	3.036	0.359	0.369	0.765	0.037
6	3.197	0.365	0.380	0.774	0.029
9	3.415	0.374	0.396	0.795	0.025
15	3.692	0.373	0.404	0.803	0.026
20	3.918	0.368	0.402	0.802	0.032
27	4.195	0.364	0.408	0.803	0.031

$\vec{c}$. With increasing pressure the two molecular pairs indicated by I_6 and I_7 move closer to each other with respect to the stacking direction $\tilde{a}$, whereas the contact I_5 develops in the opposite direction (figure 10). This results in a more parallel arrangement of the TMTTF-molecules in neighboring stacks. In contrast to the stacks linked in the b-direction, here translational-invariant TMTTF-molecules order in planes.

The pressure-induced reduction of $R_{\tilde{c}}$ for the contacts I_5 to I_7 results in a reduction of the anion cavity. The distances between anion and the methyl groups get smaller. This influences the anion and methyl group motions, as can be observed by vibrational spectroscopy [34] and magnetic measurements [35–37].

4. Band structure

The DFT calculations were based on the crystal structures obtained for different pressure values; the atomic positions were relaxed in each case. Using these relaxed structures the electronic band structures along selected lines in the Brillouin zone were calculated; the related k-space directions are visualized in figure 11. In figure 12 the electronic bands in the vicinity of the Fermi energy E_F are plotted for several pressure values P. Also indicated are the values of E_F with respect to the lowest band. In contrast to previous studies [38–40] we consider the lines in the 1st Brillouin zone as shown in figure 11.

The TMTTF salts possess a 3/4-filled conduction band (corresponding to HOMO) that is split due to the dimerization. Accordingly the electronic band structure of $(TMTTF)_2PF_2$ is characterized by a completely filled lower and a half-filled upper band. In general pressure causes a shift of the bands without significant influence on the shape of the band structure for most k-directions. Also the Fermi energy strongly increases with pressure from $E_F = 3.0359$ eV ($P = 3$ kbar) to 4.1953 eV at $P = 27$ kbar as listed in table 2. To compensate for these changes, in figure 12 the energies are given with respect to E_F. While there are only minor modifications along the chain direction ($\Gamma \to X$), there are certain directions in k-space for which important changes of the band dispersion become obvious as pressure increases; for instance $U \to V$, $V \to R$ and $R \to \Gamma$. This is best seen in figure 13 where the bands at $P = 3$ and 27 kbar are overlaid. In the following the details will be discussed.

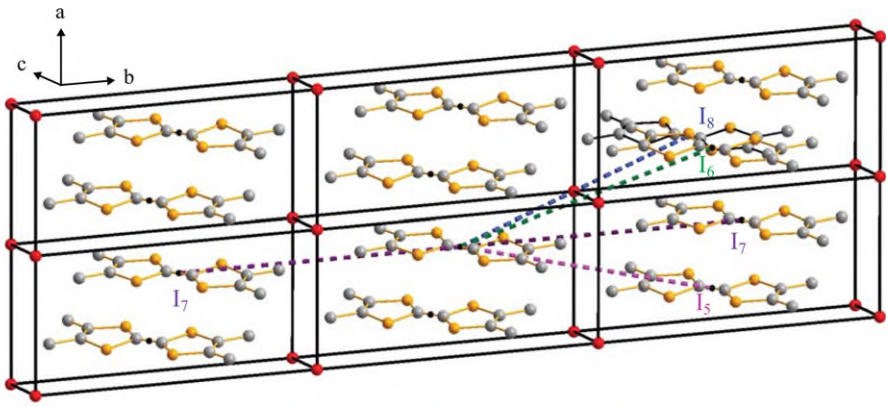

Figure 9. View of the *ac* plane of the crystal structure of $(TMTTF)_2PF_6$. Four crystallographically different neighbors can be identified in the *c*-direction, indicated by I_5, I_6, I_7 and I_8. While the TMTTF-molecules linked by I_5, I_6 and I_7 are located in neighboring unit cells shifted by the unit cell vector $\vec{c}$, the molecule connected by I_8 belongs to the next-nearest-neighbor unit cell in the direction $\vec{c}$–$\vec{b}$. These two TMTTF-molecules are related by inversion symmetry with the inversion center located at the anion position.

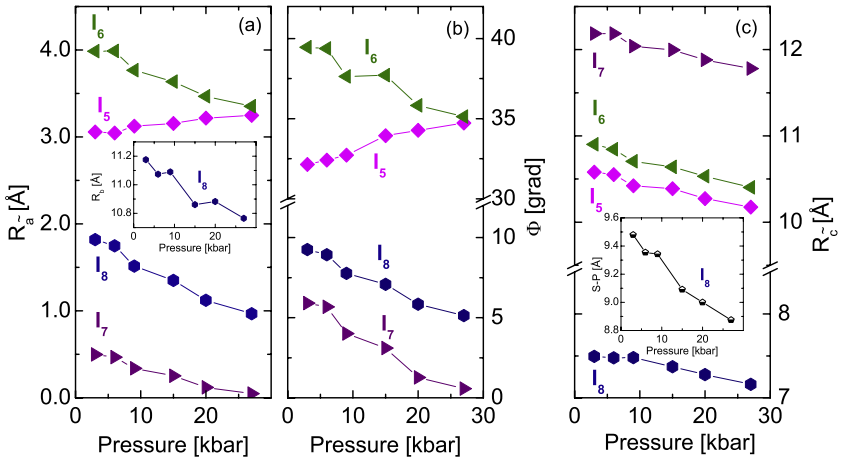

Figure 10. Changes of the distances toward the neighboring stacks in the *c*-direction. (a) Distance $R_{\tilde{a}}$ along the stacking direction. The inset presents the changes of $R_{\tilde{b}}$ under pressure for the distance I_8. For the contacts I_5 through I_7 the changes are negligible. (b) Pressure dependence of the angle Φ for the projection on the $\tilde{a}\tilde{b}$ plane. In (c) the shifts along the large molecular axis $\tilde{c}$ are shown and in the corresponding inset the distance between the sulfur atom S and the center of the anion given by P.

4.1. Changes along the stacks (a-direction)

The *k*-space direction X can be correlated with the band dispersion along the stacking direction of the TMTTF-molecules. The bandwidths of both the upper and the lower bands are rather small: 360 and 400 meV, respectively. Surprisingly the change of the bandwidth with increasing pressure is negligible. The shape of the bands remains conserved. The total bandwidth increases only by about 5% and the dimerization gap Δ_X varies slightly with pressure.

4.2. Changes toward neighboring stacks in the b-direction

The largest variations with pressure occur in the U → V direction of the *k*-space. The dispersions of both bands strongly increase (figure 13). The bandwidth almost doubles when a pressure of 27 kbar is applied (see table 3). A very prominent feature is observed in addition: a local maximum in the upper band next to the U-point. This feature points toward an eventual crossing of the Fermi level at even higher pressures. The path U → V is related to a Bragg-plane orientated parallel to the stacks ($\vec{a}$-axis) in the diagonal direction along $\vec{b}+\vec{c}$ in real space (figure 14); it is qualitatively very similar to the plane orientated perpendicular to the small molecular axis $\tilde{b}$. Thus the huge increase in dispersion for the U → V path is directly related to the changes of the overlaps of the orbitals along the small molecular axis $\tilde{b}$ (figure 8).

4.3. Changes toward neighboring stacks in the c-direction

When going from Γ → Z, X → U or V → R, each time we look along the least conducting *c*-direction with basically no appreciable band dispersion. Whereas the changes at the *k*-points Γ, Z, X and U are negligible, a pressure dependence of Δ_V and consequently of Δ_R is obvious.

Upon increase in pressure the positions of the bands at the *V*- and R-points shift, but more or less in the same way. Thus the dispersion V → R remains negligible, but the dimerization

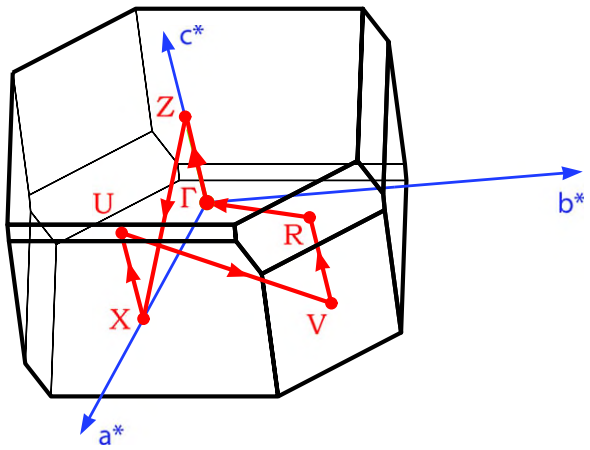

Figure 11. The first Brillouin zone of $(TMTTF)_2PF_6$. The red lines indicate the trajectories related to the performed band structure calculations, displayed in figure 12. With respect to the reciprocal primitive vectors, the points are indicated as follows: $\Gamma = (0, 0, 0)$; $Z = (0, 0, 0.5)$; $X = (0.5, 0, 0)$; $U = (0.5, 0, 0.5)$; $V = (0.5, 0.5, 0)$; $R = (0.5, 0.5, 0.5)$.

Table 3. Band structure parameters of $(TMTTF)_2PF_6$ at different pressures for the *b*-direction perpendicular to the stacks. $W_V^u = \Delta E_{U\to V}^{upper}$ and $W_V^l = \Delta E_{U\to V}^{lower}$ are the bandwidths of the upper and lower bands in the *b*-direction; Δ_V and Δ_R denote the gaps at the *V*- and R-points of the Brillouin zone, respectively. The two values in brackets describe the maximum bandwidth including the local maximum located left of the point U. The energies are listed in units of eV, the calculated error is about ±0.005 eV.

P (kbar)	W_V^u	W_V^l	Δ_V	Δ_R
3	0.143	0.134	0.029	0.035
6	0.163	0.151	0.019	0.025
9	0.181	0.166	0.011	0.013
15	0.209	0.201	0.020	0.015
20	0.219 (0.226)	0.230	0.045	0.039
27	0.240 (0.254)	0.267	0.062	0.056

gap $\Delta_V \approx \Delta_R$ changes significantly. For pressure values up to 9 kbar both gaps Δ_V and Δ_R between the lower and upper bands first shrink appreciably, whereas they start to grow and eventually double for higher pressures (table 3). The *V*- and R-points are exceptional in the Brillouin zone since they are located far away from the Γ-point.

5. Optical investigations

To compare the calculated band structures with experimental findings, high resolution angle-resolved photoelectron spectroscopy (ARPES) measurements would be the favored method as they yield the density of electronic states (DOS) as a function of momentum. In organic compounds ARPES is quite a difficult experiment due to surface problems and irradiation damage [41, 42], and it is basically impossible to perform ARPES on organic samples in a pressure cell.

Alternatively, optical spectroscopy yields valuable information on the band structure. Energy gaps due to band structure and correlations are seen by the onset of absorption; the electronic bandwidth is related to the spectral

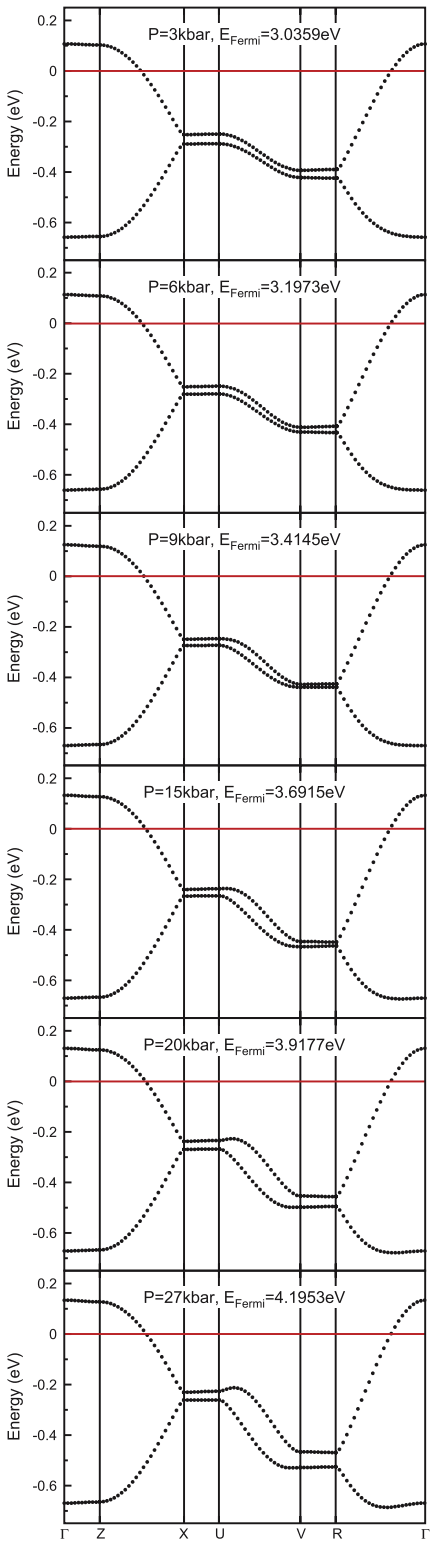

Figure 12. DFT calculations of the electronic band structure of $(TMTTF)_2PF_6$ for different pressure values ranging from 3 to 27 kbar at room temperature. The values for the pressure *P* and the Fermi energy are given for each panel. The red lines mark the Fermi energy E_F.

weight. Considering the tight-binding approximation for quasi-one-dimensional conductors

$$E(k) = E_0 + 2t_\parallel \cos\{k_\parallel d_\parallel\} + 2t_\perp \cos\{k_\perp d_\perp\}, \qquad (2)$$

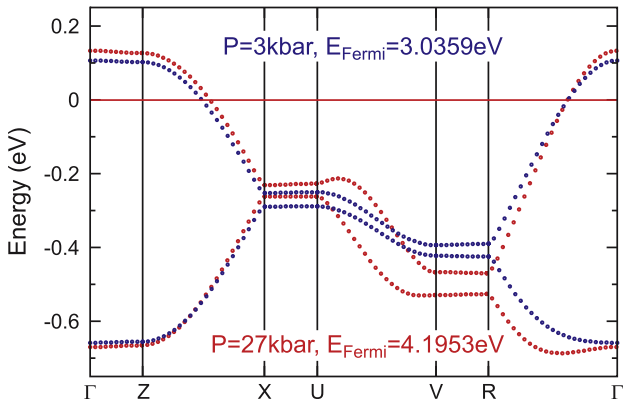

Figure 13. Comparison of the electronic band structures of $(TMTTF)_2PF_6$ calculated for the room temperature structures at pressures of $P = 3$ and 27 kbar.

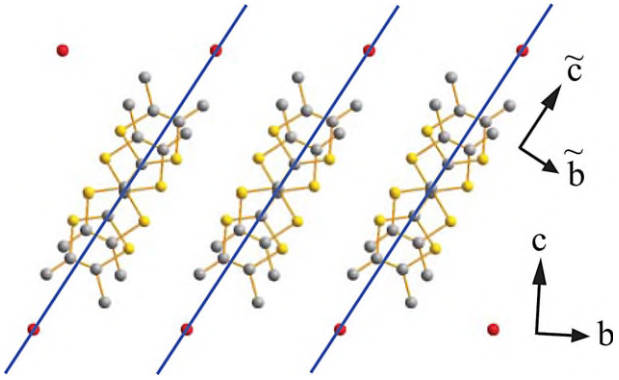

Figure 14. View along the stacking direction a onto the bc plane. Since the molecules are basically oriented along the $(\vec{b}+\vec{c})$-direction (diagonal line), the path U → V in k-space can be visualized as a Bragg-plane perpendicular to the molecular axis $\tilde{c}$ or parallel to the $\tilde{b}$-direction.

with the hopping integrals $t_\parallel$ and $t_\perp$, pointing along the a- and b'-direction respectively. In the limit of $t_\perp \ll t_\parallel$ only a warping of the Fermi surface is introduced by the small $t_\perp$ as a perturbation of the one-dimensional sheets. Then the plasma frequency is given by

$$\omega_{p\perp}^2 = \frac{2}{\pi \sin\{\rho\pi/2\}} \frac{4\pi e^2 d_\perp^2}{\hbar^2 V_m} \frac{t_\perp^2}{t_\parallel}, \tag{3}$$

where V_m is the volume per molecule, ρ is the number of electrons per site, and $d_\perp$ is the molecular distance. The bandwidth anisotropy is given by

$$\left(\frac{\omega_{p\perp}}{\omega_{p\parallel}}\right)^2 \propto \left(\frac{t_\perp}{t_\parallel}\right)^2. \tag{4}$$

Hence the spectral weight is directly related to the changes of the bandwidths W_X and W_Y by

$$\frac{\omega_{p\perp}}{\omega_{p\parallel}} \propto \frac{W_Y}{W_X}. \tag{5}$$

In order to relate the calculated band structure to experimental findings, we performed measurements of the in-

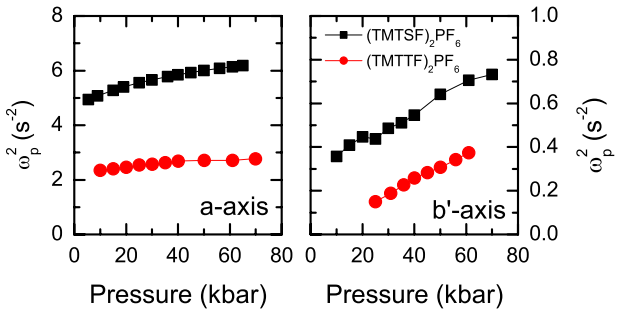

Figure 15. Pressure dependences of the plasma frequency for the a and b' directions for $(TMTTF)_2PF_6$ and $(TMTSF)_2PF_6$ obtained from room temperature measurements of the reflectivity for two different polarizations $E \parallel a$ and $E \parallel b'$. According to equation (5), ω_p is basically a measure of the bandwidth in different directions.

frared reflectivity of $(TMTTF)_2PF_6$ and $(TMTSF)_2PF_6$ under hydrostatic pressure up to 70 kbar [43–45]. From the data we extracted the optical conductivities and the spectral weights for the electric field polarized along the a and b'-directions. In figure 15 the pressure dependence of the spectral weight

$$\omega_p^2 = 8 \int \sigma_1(\omega)\, d\omega \tag{6}$$

is plotted as a function of pressure. It is obvious that the change in the a-direction for both compounds is much smaller compared to the perpendicular direction b', where the spectral weight basically quadruples when increasing the pressure up to 60 kbar. For low-pressure values $p < 20$ kbar no plasma frequency can be determined for $(TMTTF)_2PF_6$ along the b'-direction—while $\omega_{p\parallel}$ remains—indicating quasi-one-dimensionality. By applying pressure, the confinement is reduced, resulting in a finite but very low zero-energy response due to rising interchain hopping [44]. This corresponds to the pressure-induced deconfinement transition from a Mott insulator to a two-dimensional metal [46, 43]. In the case of $(TMTSF)_2PF_6$ in the perpendicular polarization metallic like conductivity is always observed, indicating a quasi-two-dimensional rather than one-dimensional physical behavior.

6. Discussion

Already from the detailed analysis of the crystallographic data we can conclude that the interstack coupling along the b-direction becomes stronger, since the distance to the neighboring TMTTF chains decreases. In addition the angle Φ changes; it accounts for the displacement of the TMTTF-molecule in adjacent stacks with respect to the b-direction, as depicted in figure 3. As a result the neighboring TMTTF-molecules arrange in a more parallel way along the b-direction, leading to a better orbital overlap between the stacks.

This evolution of the crystal structure is reflected in our band structure calculations as well. The bandwidth mainly increases along the path U → V, i.e. for the direction pointing along the b-axis. Surprisingly, the strong reduction

of the distances between the TMTTF-molecules along the stacking direction with increasing pressure does not effect the band structure significantly. The same applies for the *c*-direction. Any changes in the electronic properties along and perpendicular to the stacking direction are caused by modifications along the *b*-direction.

If interchain coupling is negligible, the strong correlation U, not taken into account in our band structure calculations, drive the system to a Mott insulator. While half-filled one-dimensional Mott systems are insulators, increasing interchain interaction reduces the Mott gap. The system develops until it crosses over to a two-dimensional metallic behavior at some critical pressure P_c [46]. This perfectly corresponds to our optical investigations under hydrostatic pressure, where we observe major changes in $E \parallel b'$ polarization. Quantitatively, this is expressed by the plasma frequency that rises linearly with pressure, as displayed in figure 15.

An indication of a dimensional crossover toward a two-dimensional system already exists in our calculated band structure. It is manifested in the local band maximum along the path U $\rightarrow$ V, indicating a possible crossing of the Fermi energy for pressures above 27 kbar. Experimentally the Mott gap is proven by the optical conductivity for light polarized along the stacking direction [44] and the increase of the spectral weight along the perpendicular direction b' points toward a deconfinement crossover. So even at low pressure this interstack coupling leads to a significant warping of the one-dimensional Fermi surface, influencing the physical properties of this system, even if the deconfinement transition is not yet achieved.

7. Summary

The pressure-dependent structure of $(TMTTF)_2PF_6$ single crystals has been investigated systematically and in detail for the first time. *Ab initio* DFT band structure calculations, taking into account the full unit cell, yield the development of the electronic band structure under pressure. The changes in crystal structure under pressure and the resulting band structure were directly related to each other. The indications for a dimensional crossover at higher pressures were compared with recent results of optical investigations at pressures up to 70 kbar.

Acknowledgments

The crystals were grown by G Untereiner. We thank D Jérome, T Knoblauch and J-P Pouget for helpful discussions. The work was supported by the Deutsche Forschungsgemeinschaft (DFG).

References

[1] Jérome D and Schulz H J 1982 *Adv. Phys.* **31** 299
[2] Jérome D 1994 *Organic Conductors* ed J-P Farges (New York: Dekker) p 405
[3] Ishiguro T, Yamaji K and Saito G 1998 *Organic Superconductors* 2nd edn (Berlin: Springer)
[4] Pouget J P and Ravy S 1996 *J. Physique* I **6** 1501
[5] Brazovskii S 2007 *The Physics of Organic Superconductors and Conductors* ed A Lebed (Berlin: Springer) p 313
[6] Dressel M 2003 *Naturwissenschaften* **90** 337
Dressel M 2007 *Naturwissenschaften* **94** 527
Dressel M 2011 *J. Phys.: Condens. Matter* **23** 293201
[7] Brown S E, Chaikin P M and Naughton M J 2007 *The Physics of Organic Superconductors and Conductors* ed A Lebed (Berlin: Springer) p 49
[8] Jérome D 1991 *Science* **252** 1509
[9] Galigne J L, Liautard B, Peytavin S, Brun G, Maurin M, Fabre J M, Torreilles E and Giral L 1979 *Acta Crystallogr.* B **34** 620
[10] Galigne J L, Liautard B, Peytavin S, Brun G, Maurin M, Fabre J M, Torreilles E and Giral L 1979 *Acta Crystallogr.* B **35** 1129
[11] Galigne J L, Liautard B, Peytavin S, Brun G, Maurin M, Fabre J M, Torreilles E and Giral L 1979 *Acta Crystallogr.* B **35** 2609
[12] Liautard B, Peytavin S, Brun G and Maurin M 1982 *Cryst. Struct. Commun.* **11** 1841
[13] Liautard B, Peytavin S, Brun G and Maurin M 1982 *Acta Crystallogr.* B **38** 2746
[14] Liautard B, Peytavin S and Brun G 1984 *Acta Crystallogr.* **C40** 1023
[15] Kobayashi H, Kobayashi A, Sasaki Y, Saito G and Inokuch H 1984 *Bull. Chem. Soc. Japan* **57** 2025
[16] Yakushi K, Aratani S, Kikuchi K, Tajima H and Kuroda H 1986 *Bull. Chem. Soc. Japan* **59** 363
[17] Granier T, Gallois B, Ducasse L, Fritsch A and Filhol A 1988 *Synth. Met.* **24** 343
[18] Thorup N, Rindorf G and Soling H 1991 *Acta Crystallogr.* B **37** 1236
[19] Gallois B, Gaultier J, Hauw C, Chasseau D, Meresse A, Filhol A and Bechgaard K 1985 *Mol. Cryst. Liq. Cryst.* **119** 225
[20] Gallois B, Gaultier J, Hauw C and Lamcharfi T-D 1986 *Acta Crystallogr.* B **42** 564
[21] Gallois B, Gaultier J, Ducasse L and Abderrabba M 1986 *Physica* B **143** 474
[22] Gallois B, Gaultier J, Lamcharfi T, Bechtel F, Filhol A, Ducasse L and Abderrabba M 1987 *Synth. Met.* **19** 321
[23] Gallois B, Gaultier J, Bechtel F, Filhol A and Vettier C 1987 *Mol. Cryst. Liq. Cryst.* **148** 279
[24] Pashkin A, Dressel M, Ebbinghaus S G, Hanfland M and Kuntscher C A 2009 *Synth. Met.* **159** 2097
[25] Köhler B, Rose E, Dumm M, Untereiner G and Dressel M 2011 *Phys. Rev.* B **84** 035124
[26] Kabsch W 1993 *J. Appl. Cryst.* **26** 795
[27] Mao H K, Xu J and Bell P M 1986 *J. Geophys. Res.* **91** 4673
[28] Giannozzi P *et al* 2009 *J. Phys.: Condens. Matter* **21** 395502
[29] Perdew J P, Burke K and Ernzerhof M 1996 *Phys. Rev. Lett.* **77** 3865
[30] Broyden C G 1965 *Math. Comput.* **19** 557
[31] Fletcher R 1970 *Comput. J.* **13** 317
[32] Goldfarb D 1970 *Math. Comput.* **24** 23
[33] Shanno D F 1970 *Math. Comput.* **24** 647
[34] Dressel M, Dumm M, Knoblauch T and Masino M 2012 *Crystals* **2** 528–78
[35] Yu W, Zang F, Zamborszky F, Alavi B, Baur A, Merlic C A and Brown S E 2004 *Phys. Rev.* B **70** 121101
[36] Salameh B, Yasin S, Dumm M, Untereiner G, Montgomery L K and Dressel M 2011 *Phys. Rev.* B **83** 205126
[37] Yasin S, Salameh B, Rose E, Dumm M, Krug von Nidda H A, Loidl A, Ozerov M, Untereiner G, Montgomery L K and Dressel M 2012 *Phys. Rev.* B **85** 144428

[38] Whangbo M H, Walsh W M, Haddon R C and Wudl F 1982 *Solid State Commun.* **43** 637
[39] Grant P M 1983 *Phys. Rev.* B **26** 6888
[40] Grant P M 1983 *J. Physique Coll.* **44** C3–847
[41] Zwick F, Brown S, Margaritondo G, Onellion M, Voit J and Grioni M 1997 *Phys. Rev. Lett.* **79** 3982
[42] Sing M, Schwingenschlogl U, Claessen R, Dressel M and Jacobsen C S 2003 *Phys. Rev.* B **67** 125402
[43] Pashkin A, Dressel M and Kuntscher C A 2006 *Phys. Rev.* B **74** 165118
[44] Pashkin A, Dressel M, Hanfland M and Kuntscher C A 2010 *Phys. Rev.* B **81** 125109
[45] Dressel M and Drichko N 2004 *Chem. Rev.* **104** 5689
[46] Giamarchi T 2004 *Quantum Physics in One Dimension* (Oxford: Oxford University Press)